Electrochimica Acta 104 (2013) 84–93

Contents lists available at SciVerse ScienceDirect

Electrochimica Acta

journal homepage: www.elsevier.com/locate/electacta

# Transient analysis through Hilbert spectra of electrochemical noise signals for the identification of localized corrosion of stainless steel

A.M. Homborg[a], T. Tinga[b], X. Zhang[c], E.P.M. van Westing[d], P.J. Oonincx[b], G.M. Ferrari[c], J.H.W. de Wit[e], J.M.C. Mol[e,*]

[a] Royal Netherlands Navy, Naval Maintenance and Sustainment Agency, P.O. Box 505, 1780AM Den Helder, The Netherlands
[b] Netherlands Defence Academy, P.O. Box 10000, 1780CA Den Helder, The Netherlands
[c] TNO Maritime Materials Performance Centre, P.O. Box 505, 1780AM Den Helder, The Netherlands
[d] Materials innovation institute (M2i) , P.O. Box 5008, 2600GA Delft, The Netherlands
[e] Delft University of Technology, Department of Materials Science and Engineering, Mekelweg 2, 2628CD Delft, The Netherlands

ARTICLE INFO

*Article history:*
Received 20 February 2013
Received in revised form 11 April 2013
Accepted 11 April 2013
Available online xxx

*Keywords:*
Electrochemical noise
Hilbert spectra
Localized corrosion
Corrosion identification

ABSTRACT

Hilbert spectra allow identification of instantaneous frequencies that are attributed to specific corrosion mechanisms in electrochemical noise data. The present work proposes to identify and analyze areas of interest in Hilbert spectra, which enables to obtain valuable frequency information from electrochemical noise signals. Experiments were performed on AISI304 exposed to aqueous HCl solutions at different pH values resulting in either distinct general or localized attack. Results indicate that application of the proposed transient analysis to Hilbert spectra provides a significantly improved determination of the frequency characteristics of the electrochemical noise signals compared to time–frequency data analysis without transient analysis.



## 1. Introduction

Corrosion processes are associated with electrochemical metal dissolution processes, causing charge transfer reactions that generate spontaneous fluctuations in current and potential. These fluctuations are detected by electrochemical noise measurements (ENM) and defined as electrochemical noise (EN). Throughout several decades, it has been the conviction of many researchers that these spontaneously occurring current and potential signatures contain valuable information about the underlying corrosion processes. In fact, the first analysis of electrochemical potential signatures and their relation with corrosion characteristics of the corroding metals was performed in the 1960s by Hagyard and Williams [1] and Iverson [2]. Hladky and Dawson [3,4] reported on their investigations on characteristic fluctuations in the electrochemical potential noise (EPN), generated by the occurrence of localized corrosion. These characteristic fluctuations are defined as transients. Transient characteristics generally indicate different corrosion mechanisms. If transients in the current are observed, these are often accompanied by transients in the potential [5,6]. Nowadays, the investigation of transients occurring in electrochemical signals due to localized corrosion processes is also reported for ENM under anodic and cathodic polarization [7–9].

The frequency contribution of each individual transient leaves a specific signature, or 'fingerprint' that can provide information on the nature of the related corrosion process. The most interesting application of ENM is the ability to identify these localized corrosion processes based on characteristic transient features, possibly the most challenging task in corrosion monitoring [10–15].

Like many natural processes, corrosion processes are typically nonstationary and nonlinear. A nonstationary process can induce a direct current (DC) drift component in an EN signal, which is, e.g. often visible by a changing mean value over time. An investigation of this DC drift component and effective trend removal techniques is presented elsewhere [16]. Commonly applied data analysis techniques like calculation of standard deviation (and noise resistance) or power spectral density of an EN signal presuppose a stationary process and require removal of this DC drift and/or windowing prior to data analysis to be effective [17–21]. Therefore, these procedures are not altogether suitable for the analysis of EN signals. Ideally, the identification of localized corrosion processes demands a data analysis procedure without the precondition of stationarity or linearity and with a high distinguishing capacity in both time and frequency domain simultaneously. Until now, the (discrete)

* Corresponding author. Tel.: +31 15 278 67 78.
*E-mail addresses:* Axel.Homborg@tno.nl (A.M. Homborg), T.Tinga@nlda.nl (T. Tinga), Xiaolong.Zhang@tno.nl (X. Zhang), E.VanWesting@m2i.nl (E.P.M. van Westing), PJ.Oonincx@nlda.nl (P.J. Oonincx), Gabriele.Ferrari@tno.nl (G.M. Ferrari), J.H.W.DeWit@tudelft.nl (J.H.W. de Wit), J.M.C.Mol@tudelft.nl (J.M.C. Mol).

0013-4686/$ – see front matter © 2013 Elsevier Ltd. All rights reserved.
http://dx.doi.org/10.1016/j.electacta.2013.04.085

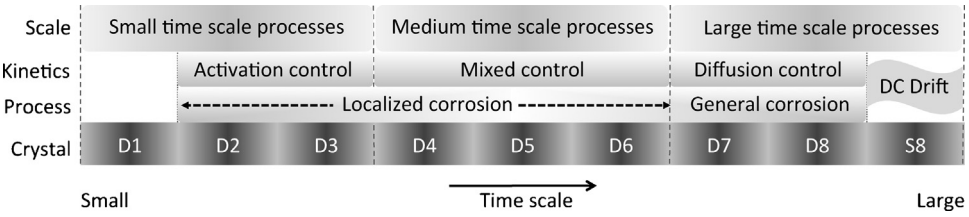


**Fig. 1.** Mechanistic information about corrosion processes that can be obtained from an energy distribution plot.

wavelet transform is the only suitable analysis technique in this respect.

Discrete wavelet transform describes the EN signal at several timescales or resolutions in so-called crystals [6,15,19,22–27]. The relative energy contributed by each crystal can be visualized in an energy distribution plot [6,19,22–28]. Such a plot provides mechanistic information about physical processes: the position of the maximum relative energy in the energy distribution plot indicates the dominant process in certain corrosion events and its change can reflect the behaviour of the dominant corrosion process [22,24,25,27,29,30]. In Fig. 1, a schematic representation of the most essential information from an energy distribution plot is provided.

Medium time scale crystals D4–D6 represent processes under mixed control (regarding localized corrosion, both diffusion and activation control can be of influence). Short timescale crystals, typically D2 and D3, are associated with activation controlled processes (these can be dominant if the localized corrosion is metastable) and large timescale crystals D7 and D8 provide information on diffusion controlled processes (dominant e.g. in the case of general corrosion, but also in the case of other large timescale processes [6,22,23,27]). In many cases the contribution of the smooth S8 crystal to the total energy is considerably large, a phenomenon that is mainly attributed to the DC drift in the original signal [6,22–24,27,28].

Contrary to the empirical mode decomposition, the alternative time–frequency method that will be used in this work, the number of iteration steps (and therefore the number of detail crystals) is user defined. It is experimentally determined that an eight-level decomposition is sufficient to capture the valuable mechanistic information in detail crystals D1–D8 [6,22–30].

For a more detailed discussion on discrete wavelet transform as performed in this work, please refer to an earlier paper by the authors [16].

An interesting alternative approach is the application of the Hilbert–Huang transform as was first proposed by Huang et al. [31]. This transform is based on the assumption that any nonlinear and nonstationary signal consists of multiple characteristic scales, or intrinsic modes of oscillation, each superpositioned on another. These so-called intrinsic mode functions are based on the local properties of the signal and can be identified empirically by their characteristic time scales through empirical mode decomposition. Unlike the wavelet transform, where wavelet crystals describe a signal on the basis of a pre-defined wavelet and using function orthogonality, here the basis is derived directly from the data itself, making the empirical mode decomposition flexible and adaptive [31–34]. A detailed description of the empirical mode decomposition and Hilbert–Huang transform procedure as performed in this work is reported by the authors in a prior work [35], where Hilbert spectra have been proposed for the analysis of EN signals under open-circuit conditions in corrosion studies. It was shown that Hilbert spectra enable a detailed determination of the instantaneous frequency composition of individual corrosion phenomena observed in the electrochemical current noise (ECN) and EPN signals at any given moment in time. This accurate fingerprinting capability enabled to identify and distinguish between different corrosion mechanisms [35]. Regarding the interpretation of EN signals, this ability makes the Hilbert–Huang transform a valuable data analysis technique.

Hilbert spectra can exhibit a significant low-frequency contribution outside the areas that are representative for transients. Such artefacts can be considered as side effects of the sifting process. The sifting process as performed in this work is described in detail elsewhere [35]. Ideally, the sifting process must satisfy two seemingly incompatible requirements to extract the intrinsic mode functions as shown in the example of Fig. 5b. First, an exact determination of instantaneous frequencies through the subsequent Hilbert–Huang transform requires the elimination of riding waves and a symmetrical wave profile of the intrinsic mode functions. For this purpose a large number of sifting iterations is preferential [36]. On the contrary, too many sifting iterations will reduce the local variations of the fluctuations under study, thereby decreasing their physical meaning. The stopping criterion for the sifting iterations thus reflects a compromise between these two opposite requirements [36]. As an example, in Fig. 5b from d8 downwards, increased amplitudes of the intrinsic mode functions outside the occurrence of a transient are observed. These generate increased amplitudes of instantaneous frequencies shown in the Hilbert spectrum of Fig. 6a, outside the areas that are reflected by the duration of the transients, and therefore outside the areas that are considered to have a physical origin.

The present work aims to illustrate that Hilbert spectra allow the identification of only the instantaneous frequency contributions that are directly related to the occurring corrosion mechanisms. The artefacts discussed before will be shown to be largely neglected by this method. The main contribution of this work is the proposal of an advanced data analysis method examining only those areas of a Hilbert spectrum where these instantaneous frequencies are present. This yields increased discrimination ability between different corrosion mechanisms as compared to discrete wavelet transform. The advantages will be demonstrated using EN data from exposure experiments of AISI304 to aqueous HCl solutions at different pH values. These experiments will generate distinctly different corrosion morphologies, ranging from general to local attack.

## 2. Experimental

### 2.1. Materials and experimental set-up

The measurements were performed in a conventional three-electrode configuration under open-circuit conditions, requiring two nominally identical stainless steel AISI304 working electrodes. The measurement setup and electrochemical cell configuration is identical to the one described earlier [35].

The working electrodes were partly coated with an epoxy primer to prevent crevice corrosion and embedded in coupons using an epoxy resin. Only a well-defined area of 0.05 $cm^2$ of each working electrode was exposed to the electrolyte. The working electrodes were wet ground using up to 4000-grit SiC paper. After

rinsing with demineralized water and microscopic inspection for irregularities they were stored under ambient conditions at 20 °C for 24 h. The reference electrode used was a Radiometer analytical Red Rod type REF201 (Ag/AgCl/sat. KCl: 0.207 V vs. SHE). The electrolytes used were aqueous HCl solutions made from demineralised water and reagent, at three different concentrations: 0.1, 0.01 and 0.001 M, corresponding with pH 1.0, 1.9 and 3.0, respectively. All solutions were open to air. The duration of each exposure to the electrolyte was 1000 s, equal to the duration of each measurement. The electrochemical cells were placed in a Faradic cage to avoid electromagnetic disturbance from external sources. The ambient temperature was controlled at 20 °C. The samples were microscopically inspected afterwards using an optical microscope with maximum magnification of 1000×. At each electrolyte concentration 9 EN measurements were performed.

Current and potential signals were recorded using a Compactstat from Ivium Technologies working as zero resistance ammeter and potentiometer, controlled by a Windows-based PC running dedicated software. The sampling frequency used for the measurements described in this work was 5 Hz. A low-pass filter of 10 Hz was applied during data recording. Instrumental noise generated by the measuring equipment is considered the only significant unwanted noise source between the Nyquist frequency (2.5 Hz here) and the cutoff frequency of the low-pass filter (10 Hz) that could cause aliasing and was therefore closely verified. This is described in more detail in a recent paper by the authors [35]. All other noise sources are expected to be well above the cutoff frequency of the low-pass filter. The maximum range of the zero resistance ammeter was set at 10 μA for the measurements in HCl at pH 1.0 and 100 nA for the other measurements, and the maximum range of the potentiometer was set at 100 mV. In order to enhance the resolution of the measured EPN signal, the initial potential is measured and subsequently electronically adjusted to zero. From then, the cell potential is measured relative to this new reference potential. This allows a narrower potential range setting of 100 mV. The increased resolution is useful in the case of transient analysis as performed in this work, where instantaneous frequencies in the mid to high frequency range can be important for the characterization of transients [35].

The data were processed using Matlab from MathWorks. The empirical mode decomposition and the Hilbert–Huang transform were calculated using a publicly available Matlab procedure from Rilling et al. [37,38].

### 2.2. Transient analysis based on Hilbert spectra

The principle of transient analysis as proposed in this work consists of two steps: identification and selection of the areas of interest in the Hilbert spectra and the subsequent analysis of the instantaneous frequencies present in these areas.

#### 2.2.1. Identification and selection of areas of interest

The first step is to identify each transient in the ECN signal in order to determine its corresponding area with instantaneous frequencies in the Hilbert spectrum. To locate transient boundaries, an understanding of the different processes reflected by the transients is important. The precise definition of the boundaries may depend on the specific features of the process and associated transient. The procedure will be demonstrated here for a typical corrosion process as investigated in this work. Fig. 2 shows an actual ECN and EPN transient in grey, extracted from the EN signals of AISI304 exposed to an aqueous HCl solution at pH 3.0, together with the adopted procedure for transient identification and selection, that will be explained in more detail at the end of this subsection.

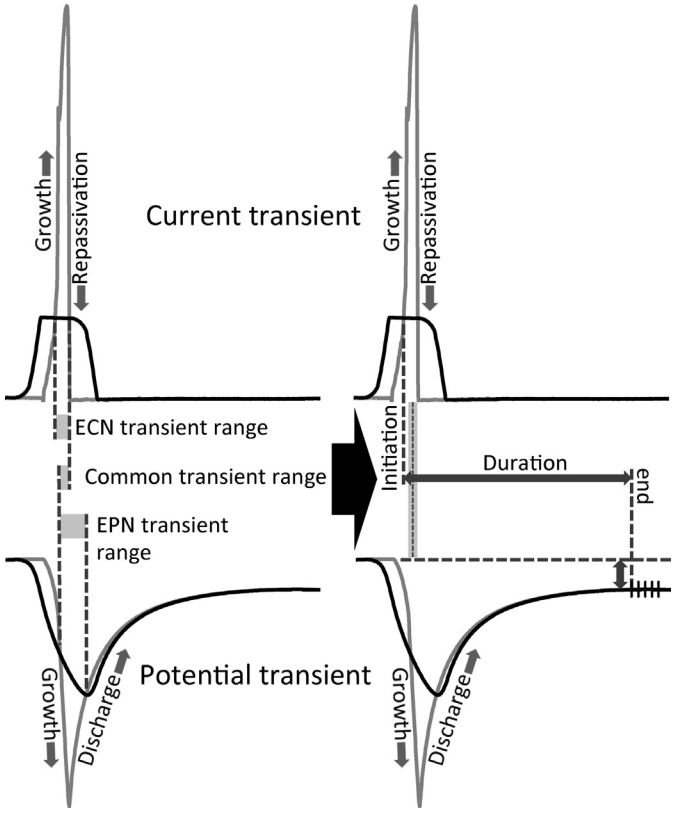


**Fig. 2.** View of ECN (top) and EPN (bottom) transients of the EN signals of AISI304 exposed to an aqueous HCl solution at pH 3.0, with their characteristic phases and a schematic representation of the procedure of identification and selection of a transient.

For the measurements carried out in this electrolyte, only metastable pitting processes were observed. Four phases can be distinguished in the transients depicted:

1. Pit initiation;
2. Metastable growth;
3. Pit repassivation;
4. Regeneration of the passive film and discharge of the interfacial capacity of the repassivated surface.

Note that the difference between the start and end point of the potential transient (indicated with the up-down arrow) is due to a gradual drift of the EPN signal during the measurement. This effect can e.g. be observed in the raw EPN signal displayed in the top graphs of Fig. 5a and b. Each couple of ECN and EPN transients represents all processes related to the lifetime of a specific metastable pit in stainless steel, from pit initiation to the final regeneration of the passive film and discharge of the interfacial capacity of the repassivated surface.

Pit initiation is indicated as the first phase of an ECN or EPN transient as the onset of metastable growth [39]. After initiation, metastable pits grow through a mechanism of undercutting the passive film [40]. Metastable growth is predominantly under diffusion control and is mainly determined by the Ohmic resistance of the perforated pit cover; i.e. its ability to withstand diffusion [40–42]. This phase is associated with the increasing magnitude of the ECN and EPN transient [39,40,43].

Repassivation takes place if the pit cover is penetrated and the pit stops growing [40]. This relatively fast process corresponds to the point where the magnitude of the ECN transient becomes zero again [39,43]. Subsequently, a discharge of the interfacial capacity

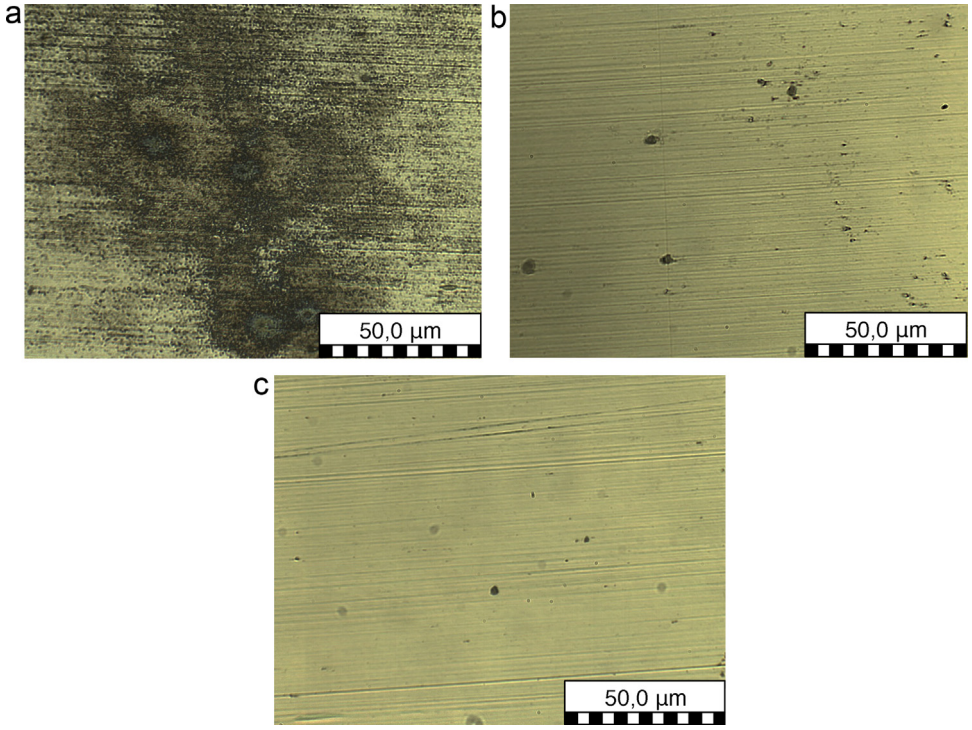


**Fig. 3.** (a) Micrograph of an AISI304 working electrode surface exposed to an aqueous HCl solution at pH 1.0 for 1000 s. (b) Micrograph of an AISI304 working electrode surface exposed to an aqueous HCl solution at pH 1.9 for 1000 s. (c) Micrograph of an AISI304 working electrode surface exposed to an aqueous HCl solution at pH 3.0 for 1000 s.

of the repassivated surface takes place and the potential recovers, reflected by the gradual decrease of the amplitude of the EPN transient towards zero [39,44].

The area of the Hilbert spectrum associated to the duration of the ECN and EPN transient couple can be regarded as representative for the processes associated with the respective metastable pit. In the case of the measurements described in this work, the first step here is to define approximate transient locations as the ranges where the absolute magnitudes of the ECN as well as the EPN signal are larger than the amplitudes of these signals after application of a moving average smoothing filter with a span of 100 data points. The left side of Fig. 2 represents this procedure. The ECN and EPN transients after the moving average smoothing filter are shown in black. This results in a set of ranges of the EN signals, equal to the number of transients present. Second, for each of these ranges the initiation and end of the associated metastable pit event is located separately. Initiation of each metastable pit event is detected as the intersection of the absolute magnitude of the ECN signal with the amplitude of the signal after application of the moving average smoothing filter. This point is defined as the starting point of the area of interest in the Hilbert spectrum. The final part of each area of interest is detected as the first location where the first derivative of 5 consecutive data points of the EPN transient crosses zero, or is equal to zero. This is schematically shown at the right hand side of Fig. 2. As such, *N* metastable pit events generate *N* areas of interest in a Hilbert spectrum.

In the absence of transients, e.g. in the case of a smooth ECN signal resulting from a general corrosion process, no areas of interest are defined and the entire Hilbert spectrum is analyzed in the next step.

### 2.2.2. Analysis of areas of interest

After discriminating the areas of interest in the Hilbert spectra, their decomposition in instantaneous frequencies must be analyzed in detail. To achieve this, first the amplitudes of the instantaneous frequencies present in these areas are normalized. The reason for this is that in some cases, artefacts (as explained in the introduction) are associated with (low) instantaneous frequencies with considerable high amplitudes, as compared to the amplitudes of instantaneous frequencies present within the areas of interest. The ability to discard artefacts present outside the areas of interest together with normalization of instantaneous frequencies inside these areas thus yields a good identification of only the frequency information of interest, while maintaining their amplitude proportions.

After discarding artefacts and normalization of the amplitudes in the Hilbert spectrum, the maxima present in all areas for each instantaneous frequency are averaged. The reason for averaging is that the amplitudes of instantaneous frequencies of some (large) transients dominate over those of others. The combination of normalization and averaging provides the required insensitivity for one or two dominant transients.

It is useful to note that the procedure of transient analysis as proposed in this work (without the final averaging) also allows investigation of the instantaneous frequency characteristics of one specific transient of interest. This ability can proof valuable in the case of in situ corrosion monitoring purposes, where the concern is mainly on the potential presence of a single pit with a large penetration. Application of the proposed transient analysis procedure to compare the instantaneous frequency characteristics of this single event with those of other localized processes present in the EN signals could yield an improved understanding of the mechanistic differences between individual localized corrosion events.

## 3. Results and discussion

In this section, first the characteristics of the corrosion processes will be discussed, after which an example of the application of transient analysis is provided. The experimental series involve AISI304 exhibiting general corrosion (pH 1.0) and localized corrosion (pH

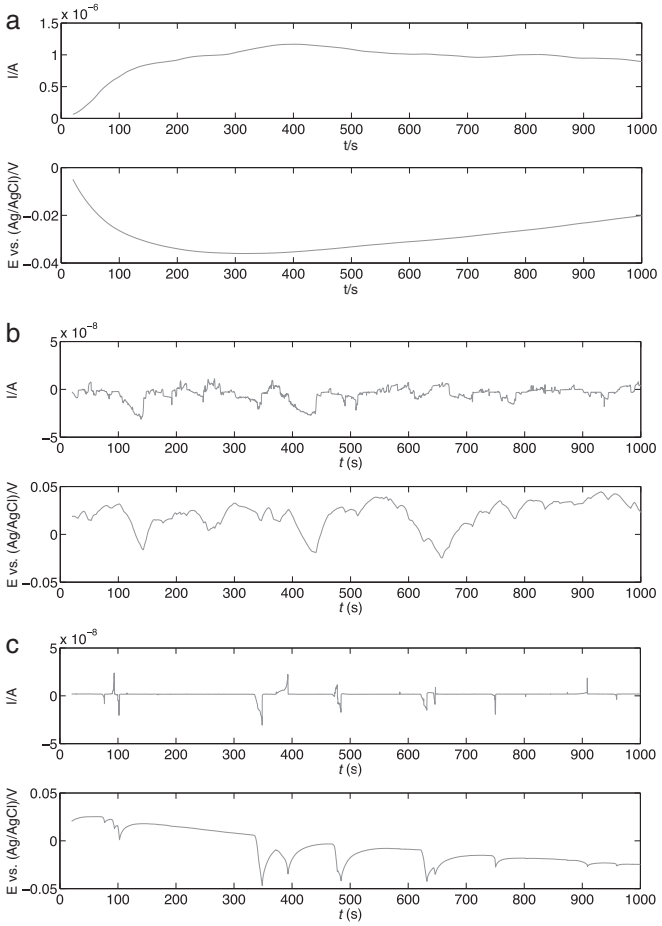


**Fig. 4.** (a) Example of an ECN and EPN signal of AISI304 exposed to an aqueous HCl solution at pH 1.0 for 1000 s. (b) Example of an ECN and EPN signal of AISI304 exposed to an aqueous HCl solution at pH 1.9 for 1000 s. (c) Example of an ECN and EPN signal of AISI304 exposed to an aqueous HCl solution at pH 3.0 for 1000 s.

1.9 and 3.0) with different corrosion behaviour in each series. Finally, the performance of the data analysis procedures is investigated based on their ability to identify and discriminate between different corrosion mechanisms.

### 3.1. Corrosion morphology

In the case of AISI304 exposed to HCl solution at three different concentrations, for each concentration different corrosion behaviour is observed. The measurements showed good reproducibility, no significant mechanistic changes were observed after repeating the measurements multiple times.

Fig. 3 shows examples of micrographs of the AISI304 working electrodes after exposure to HCl at pH 1.0 (a), 1.9 (b) and 3.0 (c) for 1000 s. In Fig. 4, example ECN and EPN signals are provided for these experiments.

The example micrograph shown in Fig. 3a is typical for a general corrosion process. It visually confirms a relatively uniformly attacked surface and some darker spots with a diameter of up to 3 μm that are more severely attacked. These spots are shallow pits, with a maximum depth of approximately 1 μm or less (determined with an optical microscope). For AISI304 in the active state, transients are not expected to be significant [45]. The current record shown in Fig. 4a is characterized by its smoothness, which is generated by the steady diffusion-controlled process [23]. In the absence of high-frequency transients, this smoothness indicates a significantly large low-frequency contribution (i.e. presence of large timescale processes) or DC drift [23,25,44,46].

Increasing the pH from 1.0 to 1.9 had a large effect on the corrosion characteristics of the AISI304 working electrodes, as is indicated in Fig. 3b, which shows an example of this. The micrograph indicates the existence of a large number of pits at the working electrode surface after the experiment, without the irregular features of general attack as was the case in the previous series. The pit depths (determined with an optical microscope) are approximately 3–4 μm. Without forming stable pits within the duration of each experiment, the large number of metastable pits generated transients in the ECN and EPN signals shown in Fig. 4b, many of them existing within the timeframe of others and as a result appearing partly superpositioned on each other in the ECN and EPN signals.

The example micrograph provided in Fig. 3c indicates a smooth working electrode surface with a smaller number of pits after 1000 s exposure to HCl solution at pH 3.0 than in the case of Fig. 3b (pH 1.9). Relating the exact amount of observed pits to the amount of transients present in the ECN or EPN signal during a single measurement at pH 3.0 is hindered, because pits sometimes become difficult to observe due to the presence of their pit cap, which forms after repassivation. The pit depths were in the order of 1–2 μm (determined with an optical microscope). In the measured ECN and EPN signals, the transients can be clearly distinguished as shown in the example signals provided in Fig. 4c. A metastable behaviour of pit initiation, limited growth and repassivation is visible and the metastable pitting phenomena are well distinguishable from each other.

### 3.2. Application of transient analysis

The procedure of identification, selection and analysis of areas of interest is illustrated by using an example ECN signal after exposure of AISI304 to an aqueous HCl solution at pH 3.0 for a duration of 1000 s.

First the wavelet and empirical mode decomposition of the ECN and EPN signals is shown in Fig. 5a and b. Fig. 5a shows an eight-level wavelet decomposition of the signals based on a Daubechies 4 wavelet and Fig. 5b shows their empirical mode decomposition. The original ECN and EPN signals are displayed at the top. Note that to enhance the resolution of the measured EPN signal, the initial potential was measured and subsequently electronically adjusted to zero. From then, the cell potential is measured relative to this new reference potential. This allows a narrower potential range setting of 100 mV.

Fig. 6 shows the Hilbert spectrum of the ECN (a) and EPN (b) signal obtained from this experiment. The original ECN and EPN signals are now displayed at the backside of the Hilbert spectra with their relative amplitudes.

In the Hilbert spectra shown in Fig. 6 multiple transients are visible, together with their decomposition in instantaneous frequencies, all with a clear localization in time. In Fig. 6a, a large low-frequency contribution at approximately $t = 300$ s can be observed. It is clear that this low-frequency information is located outside the area that is representative for the large transient starting just before $t = 350$ s. This is considered to be an example of possible artefacts arising in Hilbert spectra as explained in the introduction.

The Hilbert spectra of the EPN signals all show similar frequency characteristics, involving a relatively large low-frequency (below $10^{-2}$ Hz) part and a rapid decrease towards the higher parts of the Hilbert spectra. According to Fig. 2, the shape of an EPN transient obtained from a metastable pitting process of AISI304 is determined largely by the discharge of the interfacial capacity of the repassivated surface. This is typically a large timescale phenomenon

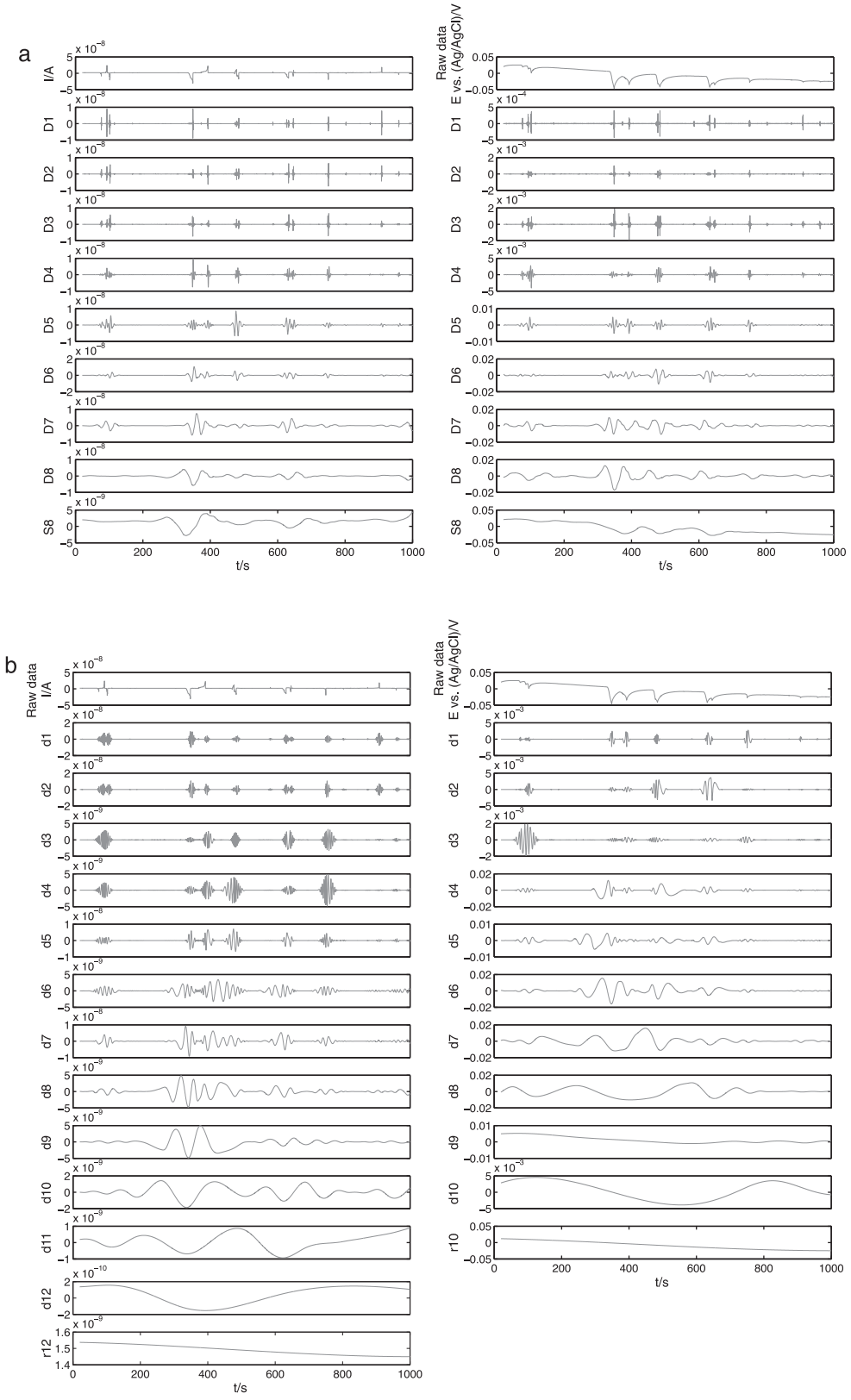


**Fig. 5.** (a) Decomposition of an original ECN and EPN signal of AISI304 exposed to an aqueous HCl solution at pH 3.0 for a duration of 1000 s into their respective detail and smooth crystals. (b) Decomposition of an original ECN and EPN signal of AISI304 exposed to an aqueous HCl solution at pH 3.0 for a duration of 1000 s into their respective detail and residual components.

resulting in a gradually decreasing magnitude of the EPN transient after each moment of repassivation. Whereas repassivation is well distinguishable in the Hilbert spectrum of an ECN signal through clearly detectable higher frequency components (between $10^{-2}$ and $10^{-1}$ Hz), the subsequent discharge of the interfacial capacity of the repassivated surface has a substantial influence on the Hilbert spectra of the EPN signal. The example Hilbert spectrum provided in Fig. 6b visualizes this: the intrinsic frequencies

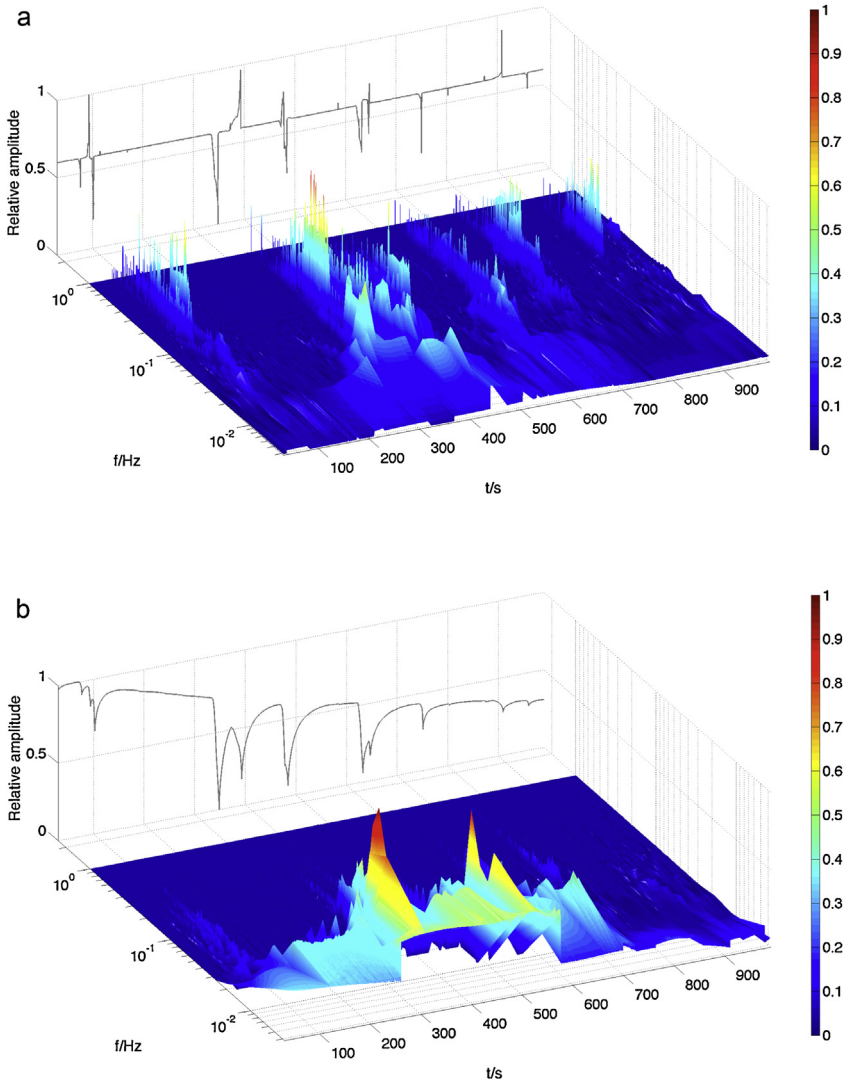


**Fig. 6.** (a) Hilbert spectrum of the ECN signal of AISI304 exposed to an aqueous HCl solution at pH 3.0 for a duration of 1000 s. (b) Hilbert spectrum of the EPN signal of AISI304 exposed to an aqueous HCl solution at pH 3.0 for a duration of 1000 s.

above approximately $10^{-2}$ Hz are small compared to the low-frequency content. Moreover, the effect of a dominating frequency contribution of one or two transients with respect to others can be observed.

The slow process of discharge of the repassivated surface takes place within the timeframe of each transient, resulting in considerable contribution of low instantaneous frequencies in each area of interest of the Hilbert spectra, for all investigated corrosion mechanisms. It is recognized that this will prevail over any low-frequency artefacts present outside the timeframes of transients. Because of this and because Hilbert spectra of the ECN signals are not affected by the capacitive discharge processes, in this work only ECN signals are investigated. These are shown to provide a good discrimination between the different corrosion processes investigated here and to reflect the rapid metastable pitting processes properly.

In order to compare the frequency information from Hilbert spectra directly to that of energy distribution plots as a reference, in this work a two-dimensional representation of the relative contributions of instantaneous frequencies in the spectrum is used. This may be best imagined as compacting the 3D spectrum into a 2D plot by removing the time axis, which allows presentation of frequency information from multiple Hilbert spectra in one plot in the next subsection.

For the example Hilbert spectrum of the ECN signal provided in Fig. 6a the two-dimensional representations of the instantaneous frequencies, with and without transient analysis, as well as the energy distribution plot, are provided in Fig. 7. In Fig. 7a, for series 1 each data point represents the average of the maxima present in all areas of interest for the respective instantaneous frequency. Series 2 shows the maxima of the instantaneous frequencies present in the entire Hilbert spectrum, including the spectrum areas between the areas of interest. Fig. 7b shows the energy distribution plot of the entire signal. The contribution of the smooth S8 crystal is subtracted from the total signal energy.

For a measurement of AISI304 exposed to HCl solution at pH 3.0, no large low-frequency contribution to the ECN signal is expected (as will be explained in Section 3.3). However, series 2 in Fig. 7a indicates the presence of a substantial low-frequency (around $10^{-2}$ Hz and lower) contribution to the overall signal. The reason for this can be found in the presence of low-frequency artefacts in this case. This indicates the advantage of the ability to ignore artefacts in the spectrum in the case of series 1 in Fig. 7a.

In addition, series 2 in Fig. 7a is mainly dominated by the contribution of instantaneous frequencies of the large transient starting just before $t = 350$ s, visible in Fig. 6a. The energy distribution plot displayed in Fig. 7b also shows this effect: the relative energy

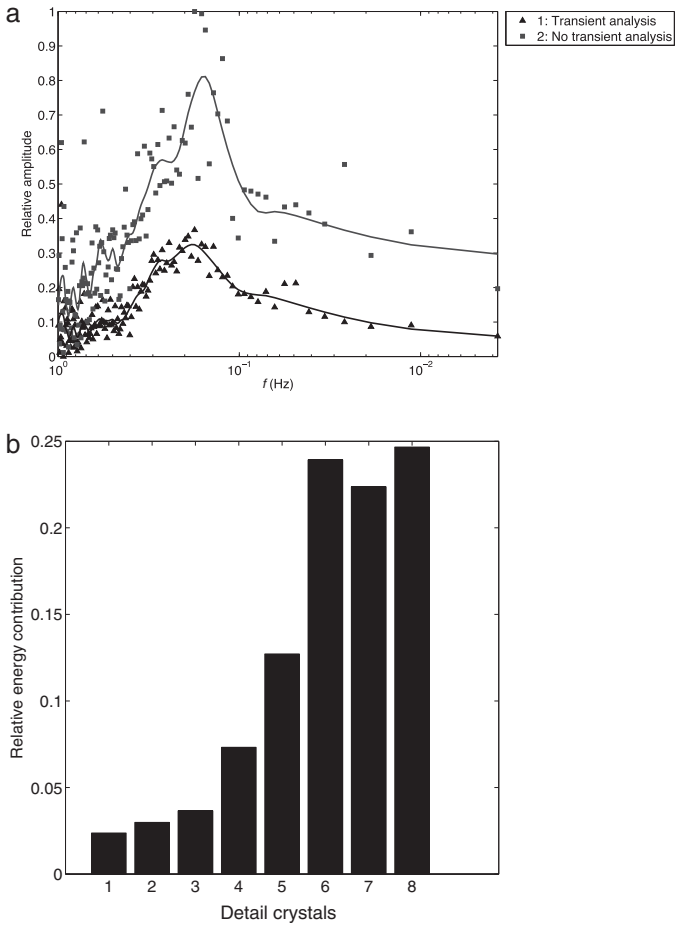


**Fig. 7.** (a) Two-dimensional representation of the Hilbert spectrum shown in Fig. 6a after transient analysis of the ECN signal (1) and without transient analysis (2). (b) Energy distribution plot of the ECN signal for the example measurement of AISI304 exposed to an aqueous HCl solution at pH 3.0 for a duration of 1000 s.

contribution of detail crystals D7 and D8 is higher than expected for this measurement. In the case of a significant difference in magnitude between individual transients, the relative energy contribution of detail crystals in the energy distribution plot is indeed likely to be dominated by the largest transient(s); discrete wavelet transform only takes into account the entire signal and does not differentiate in its spectra between individual transients (i.e. there is no time resolution). Using wavelet transform, this problem of one or two transients dominating the spectrum is therefore difficult to solve. Using Hilbert spectra, this issue is avoided by making use of their ability to distinguish the instantaneous frequency contribution of individual transients.

Summarized, the possibility provided by a Hilbert spectrum to locate the contribution of instantaneous frequencies in time enables to differentiate between areas of the spectrum that are representative for the localized corrosion processes and areas that are not. The advantage of this ability is indicated here by the difference in low frequency contribution between series 1 in Fig. 7a on the one hand and series 2 in Fig. 7a and the energy distribution plot in Fig. 7b on the other. For empirical mode decomposition, in Fig. 5b part of the low frequency information can be regarded as artefacts from the perspective of transient analysis. Furthermore, both series 2 in Fig. 7a as well as the energy distribution plot in Fig. 7b are influenced largely by the transients with the highest amplitudes. Series 1 in Fig. 7a indicates that if only instantaneous frequency information is taken into account that is located within areas of the Hilbert spectrum enclosed by the timeframes of the transients (and therefore can be regarded as representative for the corrosion process), this results in an improved accuracy of frequency information.

### 3.3. Frequency information

A discussion about the specific ability of Hilbert spectra to provide information on the corrosion characteristics of AISI304 exposed to an aqueous HCl solution at pH 1.0, 1.9 and 3.0 was reported earlier [35]. This subsection discusses the comparison between instantaneous frequency information provided by Hilbert spectra after transient analysis and without transient analysis, based on these three different measurement series. In addition, these findings will be compared to results from mechanistic information obtained from energy distribution plots.

Fig. 8a shows a two-dimensional representation of the instantaneous frequency information in Hilbert spectra after transient analysis, each time for the ECN signals of three measurements at pH 1.0, 1.9 and 3.0, respectively. Each data point represents the average of the maxima present in all areas of interest for the respective instantaneous frequency. Fig. 8b shows two-dimensional representations of the instantaneous frequency information in Hilbert spectra of the same measurements without transient analysis. Here the data points indicate the maxima of the instantaneous frequencies present in the entire Hilbert spectra. So in that case the transients have not been discriminated. Fig. 8c represents the energy distribution plots for these signals, also each time for the entire signal. The contribution of the smooth S8 crystal is each time discounted from the total signal energy.

For the measurements at pH 1.0, the two-dimensional representations of the Hilbert spectra show the presence of instantaneous frequencies only at the lowest frequency end of the spectrum, mainly below $10^{-2}$ Hz, and negligible instantaneous amplitudes in the higher frequency region. This behaviour is typical for a diffusion-controlled process, to a large extent dominated by large timescale processes [23]. Low frequency components in the ECN signal would therefore form the largest part of the Hilbert spectra along the entire time axis and, as a result, also dominate their two-dimensional representations. The Hilbert spectra shown in Fig. 8a and b are identical for these three measurements, since no transients were observed in the smooth original ECN signals. For this condition (pH 1.0), there is good correspondence between the information obtained from the Hilbert spectra shown in Fig. 8a and b and that obtained from the energy distribution plots shown in Fig. 8c. For the latter, the energy from the ECN signals is mainly located in detail crystal D8 and decreases rapidly towards shorter timescales.

By increasing the pH from 1.0 to 1.9, the Hilbert spectra of the ECN signals show an increase of activity at higher frequencies, above $10^{-2}$ Hz, which indicates the presence of a more stable passive oxide film [46]. Therefore initiation, metastable growth and repassivation of pits become visible. The relative contribution of instantaneous frequencies below $10^{-2}$ Hz (corresponding with large timescale processes) to the entire ECN signal of AISI304 has decreased in comparison to the exposure to HCl at pH 1.0, since the corrosion process is now less diffusion-controlled [23].

The two-dimensional representations of the instantaneous frequency information from the Hilbert spectra after transient analysis shown in Fig. 8a provide well-defined frequency decompositions of the ECN signals. These decompositions correspond with the expected frequency characteristics of the corrosion processes investigated here. The large number of transients present in each EN signal yields superpositioning of transients, which makes the estimation of the instantaneous frequency contribution of individual superpositioned transients less accurate. However, this inaccuracy is compensated by the large total number of transients, since the superpositioning (or overlap) occurs each time at different locations. In Fig. 8b, a large peak can be observed around $2 \times 10^{-1}$ Hz

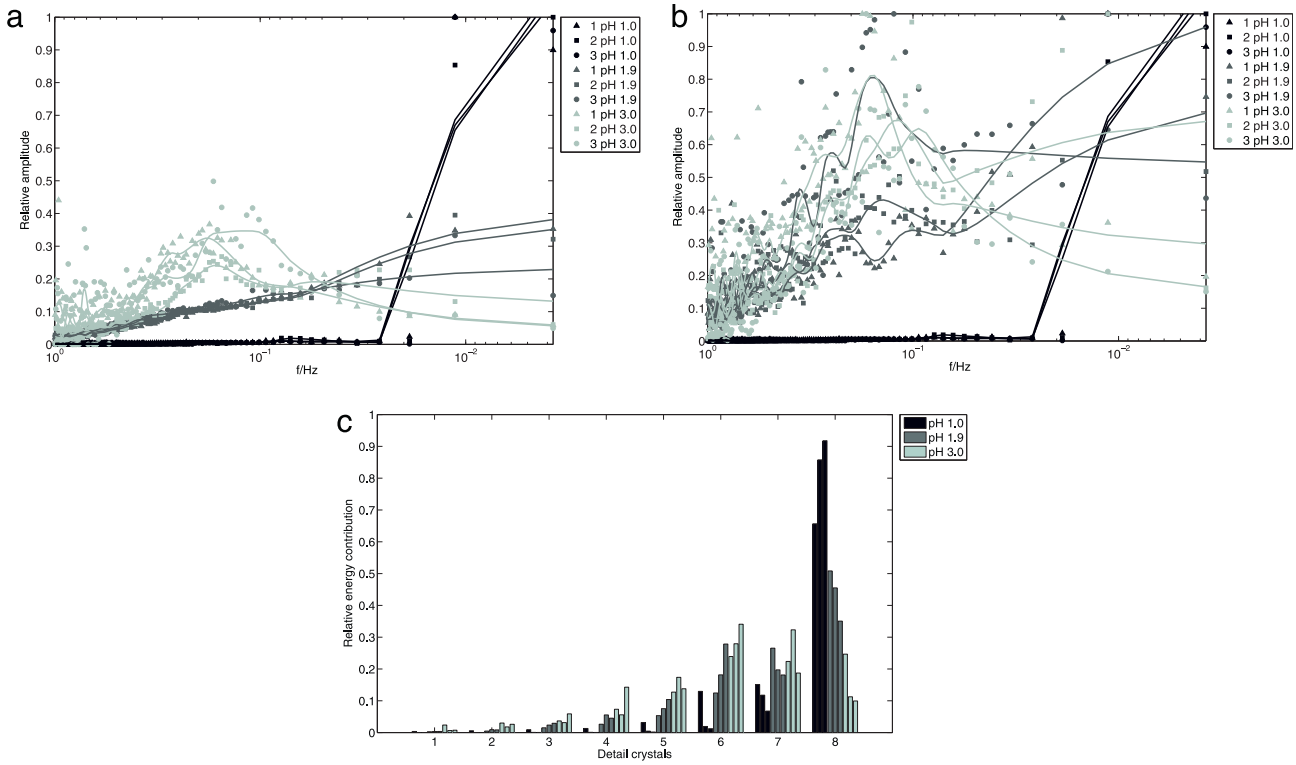


**Fig. 8.** (a) Two-dimensional representation of the Hilbert spectra after transient analysis of the ECN signals for three consecutive measurements of AISI304 exposed to an aqueous HCl solution at pH 1.0, 1.9 and 3.0 for 1000 s. (b) Two-dimensional representation of the Hilbert spectra without transient analysis of the ECN signals for three consecutive measurements of AISI304 exposed to an aqueous HCl solution at pH 1.0, 1.9 and 3.0 for 1000 s. (c) Energy distribution plots of the ECN signals for three consecutive measurements of AISI304 exposed to an aqueous HCl solution at pH 1.0, 1.9 and 3.0 for 1000 s.

in the two-dimensional representation of a Hilbert spectrum indicated with the round markers (the third series). This peak is not present after transient analysis, as shown in Fig. 8a, where the three two-dimensional representations of the Hilbert spectra all show similar frequency characteristics. In the energy distribution plot shown in Fig. 8c, this (third) measurement shows a larger relative energy contribution of detail crystal D6, as compared to the other two measurements presented. The reason for this difference can be explained by the averaging effect of transient analysis regarding the instantaneous frequency contribution of a transient with different frequency characteristics. Exceptional transients therefore have a limited effect on the final result. The two-dimensional representations of the Hilbert spectra without transient analysis and the energy distribution plots do not average these differences, but are rather influenced predominantly by the largest transients. These have a significant influence on the decomposition of the signals into their characteristic timescales for empirical mode decomposition and on the relative energy contribution of detail crystals of the signals for discrete wavelet transform. This becomes visible in Fig. 8b and c as less consistency in frequency behaviour of nominally identical measurements. In addition, this frequency behaviour is not entirely in correspondence with the expected frequency characteristics for the observed corrosion mechanisms.

The two-dimensional representations of the Hilbert spectra for the measurements at pH 3.0, provided in Fig. 8a and b, indicate a further decrease in the relative contribution of instantaneous frequencies below $10^{-2}$ Hz as compared to the Hilbert spectra of the ECN of the previous series. This is also visible in the large timescale crystals of the energy distribution plots shown in Fig. 8c as a decrease in the relative energy contribution of detail crystal D8. Hindered by an increased stability of the passive oxide film, the influence of diffusion has decreased further [23]. In addition, a clear increase of the relative contribution of instantaneous frequencies between $10^{-2}$ and $10^{-1}$ Hz can be observed, also indicating a more stable passive film [46]. The increased relative energy contribution of medium timescale crystals D5, D6 and, to a less extent, D3 and D4, in the energy distribution plots shown in Fig. 8c corresponds with this observation.

Although the Hilbert spectra and energy distribution plots show similar frequency characteristics of the corrosion phenomena, the ability of the Hilbert spectra to differentiate between individual transients proves to be an important advantage. The expected frequency characteristics of the measurements investigated here are best reflected by the two-dimensional representations of the instantaneous frequency information from the Hilbert spectra after transient analysis shown in Fig. 8a. By considering only the instantaneous frequency contribution that can be regarded as representative for the localized corrosion processes (i.e. applying transient identification, selection and analysis) instead of investigating the entire signal, the measurements investigated in this work could be decomposed in distinct and well-recognizable instantaneous frequencies. This yields an improved discrimination between different corrosion characteristics as compared to the energy distribution plot.

## 4. Conclusions

The advantage of Hilbert spectra to locate the instantaneous frequency contribution of individual localized corrosion phenomena in time has been demonstrated in earlier work of the authors [35]. The present work has shown that investigation of two-dimensional representations of the specific areas of interest in these Hilbert spectra in most cases provided an accurate and robust description of the characteristic frequency properties of localized corrosion processes occurring during the experiments investigated here.

The method as proposed here for transient identification and selection of AISI304, used to select specific areas of the Hilbert spectra that can be regarded as representative for localized corrosion processes, enables to discriminate between valuable frequency information and probable artefacts. Application of the method was shown to yield an improved definition of frequency characteristics of different corrosion mechanisms. Experiments were performed involving three well-known corrosion processes, exposing AISI304 in aqueous HCl solutions at different pH values. The frequency characteristics visible in two-dimensional representations of the Hilbert spectra of the ECN signals after transient analysis proved to be more consistent with the theoretically expected frequency contribution of corrosion mechanisms than information obtained from a similar analysis without transient analysis. Comparison with the information obtained from energy distribution plots based on wavelet transform confirmed the increased accuracy of the proposed transient analysis.

## Acknowledgements

The Naval Maintenance and Sustainment Agency of the Royal Netherlands Navy and TNO Maritime Materials Performance Centre are gratefully acknowledged for enabling this research and accommodating the research work, respectively. This research was carried out under project number M32.6.10396 in the framework of the Research Programme of the Materials innovation institute M2i (http://www.m2i.nl).

## References

[1] T. Hagyard, J.R. Williams, Potential of aluminium in aqueous chloride solutions. Part 1, Transactions of the Faraday Society 57 (1961) 2288–2294.
[2] W.P. Iverson, Transient voltage changes produced in corroding metals and alloys, Journal of the Electrochemical Society 115 (1968) 617–618.
[3] K. Hladky, J.L. Dawson, The measurement of localized corrosion using electrochemical noise, Corrosion Science 21 (1981) 317–322.
[4] K. Hladky, J.L. Dawson, The measurement of corrosion using electrochemical 1/*f* noise, Corrosion Science 22 (1982) 231–237.
[5] S.-W. Kim, H.-P. Kim, Electrochemical noise analysis of PbSCC of alloy 600 SG tube in caustic environments at high temperature, Corrosion Science 51 (2009) 191–196.
[6] T. Zhang, Y. Shao, G. Meng, F. Wang, Electrochemical noise analysis of the corrosion of AZ91D magnesium alloy in alkaline chloride solution, Electrochimica Acta 53 (2007) 561–568.
[7] H.S. Klapper, J. Goellner, A. Heyn, The influence of the cathodic process on the interpretation of electrochemical noise signals arising from pitting corrosion of stainless steels, Corrosion Science 52 (2010) 1362–1372.
[8] J.J. Kim, Wavelet analysis of potentiostatic electrochemical noise, Materials Letters 61 (2007) 4000–4002.
[9] C. Aldrich, B.C. Qi, P.J. Botha, Analysis of electrochemical noise data with phase space methods, Minerals Engineering 19 (2006) 1402–1409.
[10] R.A. Cottis, Simulation of electrochemical noise due to metastable pitting, Journal of Corrosion Science and Engineering 3 (2000) 1–9.
[11] S.V. Muniandy, W.X. Chew, C.S. Kan, Multifractal modelling of electrochemical noise in corrosion of carbon steel, Corrosion Science 53 (2011) 188–200.
[12] C. Gabrielli, M. Keddam, Review of applications of impedance and noise analysis to uniform and localized corrosion, Corrosion 48 (1992) 794–811.
[13] M. Breimesser, S. Ritter, H. Seifert, T. Suter, S. Virtanen, Application of electrochemical noise to monitor stress corrosion cracking of stainless steel in tetrathionate solution under constant load, Corrosion Science 63 (2012) 129–139.
[14] Q. Hu, G. Zhang, Y. Qiu, X. Guo, The crevice corrosion behaviour of stainless steel in sodium chloride solution, Corrosion Science 53 (2011) 4065–4072.
[15] A. Aballe, M. Bethencourt, F.J. Botana, M. Marcos, J.M. Sánchez-Amaya, Use of wavelets to study electrochemical noise transients, Electrochimica Acta 46 (2001) 2353–2361.
[16] A.M. Homborg, T. Tinga, X. Zhang, E.P.M. van Westing, P.J. Oonincx, J.H.W. de Wit, J.M.C. Mol, Time–frequency methods for trend removal in electrochemical noise data, Electrochimica Acta 70 (2012) 199–209.
[17] R.A. Cottis, Interpretation of electrochemical noise data, Corrosion 57 (2001) 265–285.
[18] F. Mansfeld, Z. Sun, C.H. Hsu, A. Nagiub, Concerning trend removal in electrochemical noise measurements, Corrosion Science 43 (2001) 341–352.
[19] Z. Dong, X. Guo, J. Zheng, L. Xu, Calculation of noise resistance by use of the discrete wavelets transform, Electrochemistry Communications 3 (2001) 561–565.
[20] U. Bertocci, F. Huet, R.P. Nogueira, P. Rousseau, Drift removal procedures in the analysis of electrochemical noise, Corrosion 58 (2002) 337–347.
[21] B.D. Malamud, D.L. Turcotte, Self-affine time series: measures of weak and strong persistence, Journal of Statistical Planning and Inference 80 (1999) 173–196.
[22] F.H. Cao, Z. Zhang, J.X. Su, Y.Y. Shi, J.Q. Zhang, Electrochemical noise analysis of LY12-T3 in EXCO solution by discrete wavelet transform technique, Electrochimica Acta 51 (2006) 1359–1364.
[23] B. Zhao, J.-H. Li, R.-G. Hu, R.-G. Du, C.-J. Lin, Study on the corrosion behavior of reinforcing steel in cement mortar by electrochemical noise measurements, Electrochimica Acta 52 (2007) 3976–3984.
[24] A.-M. Lafront, F. Safizadeha, E. Ghali, G. Houlachi, Study of the copper anode passivation by electrochemical noise analysis using spectral and wavelet transforms, Electrochimica Acta 55 (2010) 2505–2512.
[25] A. Aballe, M. Bethencourt, F.J. Botana, M. Marcos, Using wavelets transform in the analysis of electrochemical noise data, Electrochimica Acta 44 (1999) 4805–4816.
[26] A. Aballe, M. Bethencourt, F.J. Botana, M. Marcos, Wavelet transform-based analysis for electrochemical noise, Electrochemistry Communications 1 (1999) 266–270.
[27] C. Cai, Z. Zhang, F. Cao, Z. Gao, J. Zhang, C. Cao, Analysis of pitting corrosion behavior of pure Al in sodium chloride solution with the wavelet technique, Journal of Electroanalytical Chemistry 578 (2005) 143–150.
[28] Z.-N. Yang, Z. Zhang, W.-H. Leng, K. Ling, J.-Q. Zhang, In-situ monitoring of nickel electrodeposit structure using electrochemical noise technique, Transactions of Nonferrous Metals Society of China 16 (2006) 209–216.
[29] M. Shahidi, S.M.A. Hosseini, A.H. Jafari, Comparison between ED and SDPS plots as the results of wavelet transform for analyzing electrochemical noise data, Electrochimica Acta 56 (2011) 9986–9997.
[30] Y. Li, R. Hu, J. Wang, Y. Huang, C.-J. Lin, Corrosion initiation of stainless steel in HCl solution studied using electrochemical noise and in-situ atomic force microscope, Electrochimica Acta 54 (2009) 7134–7140.
[31] N.E. Huang, Z. Shen, S.R. Long, M.C. Wu, H.H. Shih, Q. Zheng, N.C. Yen, C.C. Tung, H.H. Liu, The empirical mode decomposition and the Hilbert spectrum for nonlinear and non-stationary time series analysis, Proceedings of the Royal Society of London 454 (1998) 903–995.
[32] N.E. Huang, Z. Shen, S.R. Long, A new view of nonlinear water waves: the Hilbert spectrum, Annual Review of Fluid Mechanics 31 (1999) 417–457.
[33] Z. Wu, N.E. Huang, A study of the characteristics of white noise using the empirical mode decomposition method, Proceedings of the Royal Society of London 460 (2004) 1597–1611.
[34] M. Feldman, Hilbert transform in vibration analysis, Mechanical Systems and Signal Processing 25 (2011) 735–802.
[35] A.M. Homborg, E.P.M. van Westing, T. Tinga, X. Zhang, P.J. Oonincx, G.M. Ferrari, J.H.W. de Wit, J.M.C. Mol, Novel time–frequency characterization of electrochemical noise data in corrosion studies using Hilbert spectra, Corrosion Science 66 (2013) 97–110.
[36] N.E. Huang, M.C. Wu, S.R. Long, S.S.P. Shen, W. Qu, P. Gloersen, K.L. Fan, A confidence limit for the empirical mode decomposition and Hilbert spectral analysis, Proceedings of the Royal Society of London 459 (2003) 2317–2345.
[37] G. Rilling, P. Flandrin, P. Goncalves, On empirical mode decomposition and its algorithms, in: IEEE-EURASIP Workshop on Nonlinear Signal and Image Processing NSIP-03, Grado, Italy, 2003, pp. 1–5.
[38] P. Flandrin, G. Rilling, P. Goncalves, Empirical mode decomposition as a filter bank, IEEE Signal Processing Letters 11 (2004) 112–114.
[39] G. Berthomé, B. Malki, B. Baroux, Pitting transients analysis of stainless steels at the open circuit potential, Corrosion Science 48 (2006) 2432–2441.
[40] G.S. Frankel, L. Stockert, F. Hunkeler, H. Boehni, Metastable pitting of stainless steel, Corrosion 43 (1987) 429–436.
[41] P.C. Pistorius, G.T. Burstein, Growth of corrosion pits on stainless steel in chloride solution containing dilute sulphate, Corrosion Science 33 (1992) 1885–1897.
[42] G.T. Burstein, P.C. Pistorius, S.P. Mattin, The nucleation and growth of corrosion pits on stainless steel, Corrosion Science 35 (1993) 57–62.
[43] M.G. Pujar, U. Kamachi Mudali, S.S. Singh, Electrochemical noise studies of the effect of nitrogen on pitting corrosion resistance of high nitrogen austenitic stainless steels, Corrosion Science 53 (2011) 4178–4186.
[44] J.A. Wharton, R.J.K. Wood, B.G. Mellor, Wavelet analysis of electrochemical noise measurements during corrosion of austenitic and superduplex stainless steels in chloride media, Corrosion Science 45 (2003) 97–122.
[45] E.F.M. Jansen, Pitting corrosion of stainless steels: the role of inclusions and the effect of surface deformation, Delft University of Technology, Ph.D. thesis, 1993.
[46] H.S. Klapper, J. Goellner, Electrochemical noise from oxygen reduction on stainless steel surfaces, Corrosion Science 51 (2009) 144–150.